

# Self-tracking high-resolution wide-field OCT angiography

XIANG WEI,<sup>1,2</sup> TRISTAN T. HORMEL,<sup>1</sup> YUKUN GUO,<sup>1</sup> THOMAS S. HWANG<sup>1</sup>  
AND YALI JIA<sup>1,2\*</sup>

<sup>1</sup>Casey Eye Institute, Oregon Health & Science University, Portland, Oregon, 97239, USA

<sup>2</sup>Department of Biomedical Engineer, Oregon Health & Science University, Portland, Oregon, 97239, USA

[\\*jiaya@ohsu.edu](mailto:jiaya@ohsu.edu)

**Abstract:** In this study, we demonstrate a novel self-tracking method that suppresses eye motion and blinking artifacts on wide-field optical coherence tomographic angiography (OCTA) without requiring any hardware modification. Highly efficient GPU-based, real-time OCTA image acquisition and processing software was developed to detect eye motion artifacts. The algorithm includes an instantaneous motion index that evaluates the strength of motion artifact on *en face* OCTA images. Areas with suprathreshold motion and eye blinking artifacts are automatically rescanned in real-time. Both healthy eyes and eyes with diabetic retinopathy were imaged using this system, and the tracking system can remove the blinking artifacts and large motion.

© 2019 Optical Society of America under the terms of the [OSA Open Access Publishing Agreement](#)

## 1. Introduction

Optical coherence tomography (OCT) is a non-invasive modality capable of detailed imaging of retinal and choroidal structure [1]. OCT can also produce angiographic data (OCTA) by measuring motion contrast between successive OCT images [2-5]. Compared to conventional angiographic imaging techniques such as fluorescein angiography (FA), OCTA provides superior resolution as well as volumetric data [6]. As a non-invasive imaging method, OCTA also avoids the potential side effects and discomfort associated with dye injection [6].

Wide-field OCTA imaging has recently attracted significant research interest. Some diseases, like diabetic retinopathy (DR), can manifest with predominantly peripheral vascular changes not visible in typical OCTA macular scans [7]. While it has a wider field-of-view (FOV) than OCTA, because of potential side effects FA is not considered suitable for routine imaging [8]. In contrast, wide-field OCT- which is faster, safer, and more comfortable for the patient- could be used in routine settings. Wide-field OCT has been implemented in studies since 2010, but it has been limited by lower resolution [9]. With improvement in laser sweep-rate and image processing techniques, several groups have explored high-resolution wide-field OCTA [10-12]. To maintain comparable image resolution with a larger FOV, the total number of sampling points needs to be greatly increased along both the fast and slow axes. Typically, the sampling density should meet the Nyquist criterion. This results in longer inter-frame and total imaging times, which in turn exacerbates artifacts due to microsaccade motion, blinking, and tear film evaporation [13]. Hardware improvements can yield high-resolution, large FOV OCTA simply by increasing scan rate [11, 14], and many groups have developed such fast-scanning systems [14-17]. Still, even in state-of-the-art systems, data acquisition requires some trade-off between image resolution and FOV size [11].

Successful widefield systems, therefore, require some means of artifact minimization. Broadly, two approaches are postprocessing [18] and real-time elimination of artifacts. Postprocessing algorithms can be used to suppress certain artifacts [19]. However, postprocessing corrections involve some degree of information loss [18] and may require multiple volume acquisitions, thereby increasing the total imaging time [20]. Montaging

combines real-time acquisition with post processing to produce large FOV OCTA images. [20, 21]. However, image stitching can introduce new artifacts while simultaneously increasing acquisition time and difficulty [22].

An alternative approach to artifact minimization is to use real-time blink and motion artifact correction [23]. Many prototypes [23-25] and commercial OCT systems like the RTVue (Optovue Inc., USA), CIRRUS (Carl Zeiss AG, Germany) and Spectralis (Heidelberg Engineering, Germany) already incorporate motion tracking. Currently, such eye motion tracking systems are based on allied imaging methods, like infrared fundus photography or scanning laser ophthalmoscopy (SLO) [23-25]. These systems require additional imaging hardware in the OCT optical axis to simultaneously acquire images. Such schemes have several drawbacks. Both fundus camera and SLO images need to be acquired and processed separately from the OCT image, increasing the processing requirements of the system [23]. In addition, SLO and fundus photography can only provide indirect information about the OCT image quality. Finally, more complex OCT system can increase the cost of the system and make maintenance and repair more difficult. A tracking method that does not require additional hardware can obviate these problems. One possible solution is a tracking method directly based on OCTA, which often already calculates decorrelation [3] that can be used to detect motion. Here, we introduce a novel OCTA based self-tracking method that can efficiently remove motion and blinking artifacts.

## 2. Method

### 2.1 400 kHz swept-source OCT (SS-OCT) system

This system uses a customized 400-kHz swept-source laser (Axsun Technologies, USA), which is 4-6 times faster than the laser used in commercially available devices. The laser has a center wavelength of 1060 nm with 100 nm sweep range operating at 100% duty cycle. The maximum theoretical axial resolution is 4  $\mu\text{m}$  in tissue [26]. With an appropriate optical design of the sample arm we recently reported [11] that a 75-degree maximum FOV can be achieved. Different from our previously study, the spot size on the retina was reduced to 10  $\mu\text{m}$ , which is equivalent to the maximum lateral resolution that this system can achieve.

### 2.2 GPU based real-time OCT/OCTA

We developed GPU-based real-time OCT/OCTA data acquisition and processing software for swept-source OCT system modified from our previous study [27]. The split-spectrum amplitude-decorrelation angiography (SSADA) algorithm was applied to compute OCTA flow signal [3]. SSADA increases the flow signal-to-noise ratio by combining flow information from each split-spectrum. GPU-based parallel data processing further improves real-time efficiency [27] by processing the OCT and OCTA images in a single GPU thread (Fig. 1). For each processing batch, the fast Fourier transform is only applied once to minimize the processing time. One of the major problems for real-time processing is the data transfer speed, which for many tasks (including OCT and OCTA image generation) is lower than the processing speed. In contrast to our previous work, to reduce data transfer time, 12 B-scans at four locations were batched for each transfer. The total processing and transfer time for each batch is less than 30 ms, lower than the acquisition time of 42 ms for 12 B-scans. The mean values of OCT and OCTA cross-sectional images are projected to generate OCT and OCTA *en face* images. Both cross-sectional and *en face* images are displayed on a custom graphical user interface (GUI) in real-time.

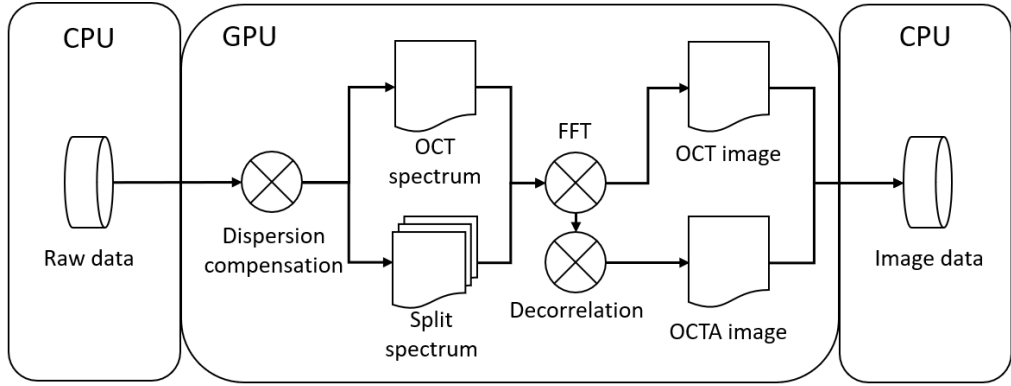


Figure 1, Flow chart showing GPU based real-time OCT/OCTA image processing. The raw spectrum is first transferred from the CPU memory to the GPU memory, and a GPU based dispersion compensation algorithm is then applied to the raw spectrum. Both the full OCT spectrum and split-spectrums for SSADA are processed using a Fast Fourier Transform (FFT). The OCT image is generated immediately after the FFT, while OCTA is generated after application of a decorrelation algorithm. In the last step, all the images are transferred back to CPU memory.

### 2.3 Self-tracking OCT/OCTA

Conventional eye motion tracking algorithms are based on the correlation between two sequentially acquired fundus *en face* images either from infrared camera or SLO. The information used to calculate correlation is mainly from the major retinal vasculature. This procedure requires additional hardware and software support. OCTA generates vasculature and motion signal itself; therefore, it is natural to use the OCTA signal for tracking. To better represent the motion strength, we defined an instantaneous motion strength index (IMSI) using the normalized standard deviation of the *en face* OCTA data:

$$\text{IMSI} = \frac{\text{std}(D_{\text{OCTA}})}{\text{mean}(D_{\text{OCTA}})} \quad (1)$$

$D_{\text{OCTA}}$  represents the mean projection *en face* OCTA image values generated from single batched raw data (12 B-scans). The MSI was calculated in a single CPU thread after the OCTA *en face* image is generated in the GPU. A global threshold is set to highlight all involuntary motion and microsaccades. The performance of this motion index was evaluated using wide-field *en face* OCTA images generated in real-time from a healthy human volunteer (Figure 2).

Besides the detection of microsaccades, blink detection is also required to achieve artifact-free OCTA imaging. During high-resolution wide-field OCTA image acquisition with our system, the imaging subject can freely blink several times in order to keep the tear film intact. During the blinking time course, the signal strength is significantly reduced. One straightforward approach for blink detection is to set a secondary threshold on the signal strength of the OCT structural image. When the signal strength is lower than the threshold, a blink may be detected. However, this approach may cause many false detections during wide-field imaging. A major artifact source in wide-field OCT image is shadow artifacts caused by vignetting and vitreous opacity, which frequently occur in wide FOV imaging and significantly reduce signal strength. The tracking system can mistake the signal strength decrease caused by shadow artifacts as a blink. However, at the initiation of a blink, the eye usually has a large axial movement, which can be detected by IMSI. When the eye is closed, the OCTA signal has low variation, and the IMSI value is low across an entire batch. The IMSI calculated from combining the batch at the blink initiation and eye closure will yield a high value, indicating blinking artifacts. In our motion and blink detection mechanism, the IMSI is a normalized metric, independent of the variation of OCTA signal strength. This fixed IMSI threshold can be used across different imaging subjects and different systems. After correctly detecting the

motion and blink artifacts, the system then automatically rescans the artifact-affected areas to restore image quality.

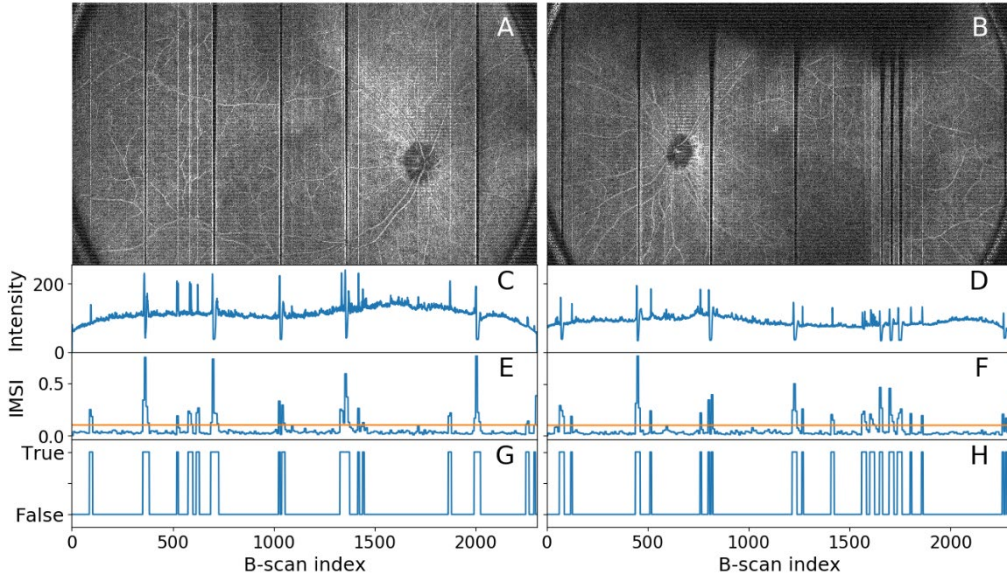


Figure 2, (A, B) OCTA mean projection *en face* images acquired from a healthy volunteer without the tracking system engaged, (C, D) mean values from each OCTA B-frame (E, F) IMSI calculated using the *en face* OCTA image, with yellow line indicating the threshold, (G, H) motion trigger signal generated after the threshold applied to the IMSI value.

#### 2.4 Cross scanning pattern for alignment

Wide-field OCT/OCTA image acquisition requires highly accurate alignment. Effectively avoiding vignetting artifacts can increase the image quality. To help the OCTA operator align the OCT axis to the eye we applied a cross scanning pattern that shows both horizontal and vertical scans at the same time (Figure 3). The scanning pattern contains 4 individual sections, one horizontal scan, one vertical scan, and two fly-back scans. Each of these scans can be used to generate OCT images. In our application, only the horizontal scan and the vertical scan are displayed. By using these two orthogonal scans, the OCT operator can effectively adjust the horizontal and vertical position to avoid shadow artifacts from misalignment.

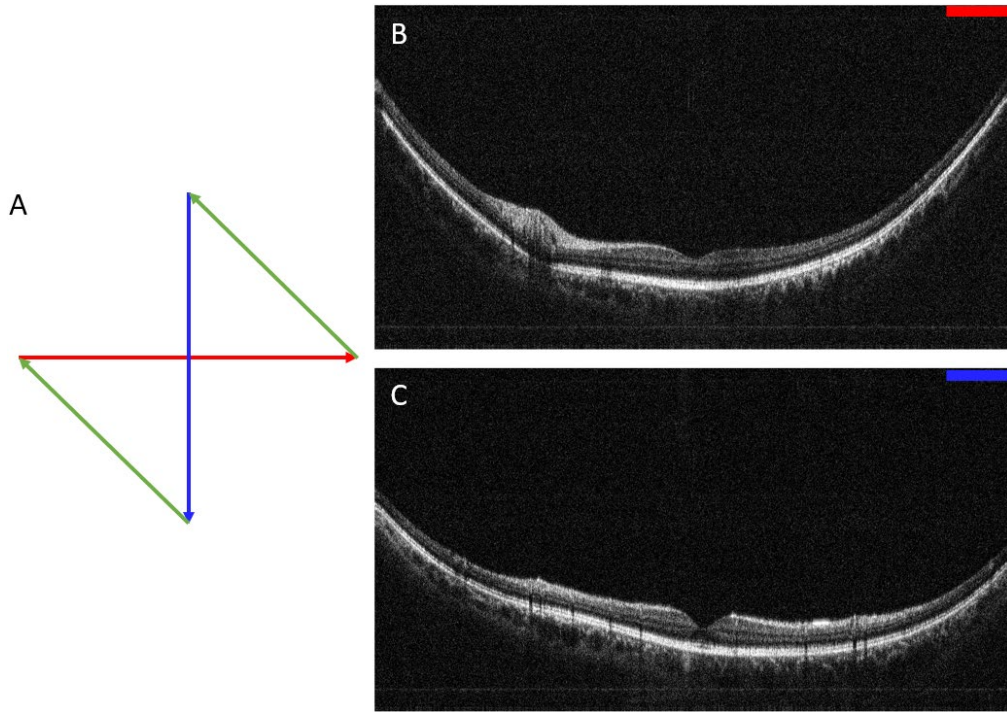


Figure 3, (A) diagram of the cross-scanning pattern. Red indicates the horizontal scan path, blue indicates the vertical scan path, and green indicates the scanner reset path, (B) horizontal cross-sectional image, (C) vertical cross-sectional image.

### 3. Results

#### *Healthy human*

To evaluate performance of the tracking system, we applied our algorithm with different scanning patterns on both a healthy volunteer and a DR patient. First, we acquired two wide-field high-resolution OCTA images from a healthy human volunteer, once without (Fig 4A) and once with (Fig 4B) the tracking system. For each volume, images contained 2560 A-lines per B-scan and 1920 B-scans per volume, with two repeats. The sampling step size in the fast axis was 9  $\mu\text{m}$  and in the slow axis was 12  $\mu\text{m}$ . The total data acquisition time was 25 seconds without tracking. In this work, the total scanning time of the image with tracking was always less than 1 minute. During the data acquisition with tracking, when the volunteer blinked their eyes, the system successfully detected each blink and rescanned the area right after the eye reopened. Motion artifacts were also successfully detected each time. Large motion artifacts were successfully removed; however, in order to complete the scan within a reasonable time (<1 min), some very mild motion artifacts that were lower than the IMSI threshold were intentionally not detected. The inner retina OCTA image was generated after layer segmentation [28] using maximum projection [29]. A Gabor filter, histogram equalization, and a custom color map were applied for display.

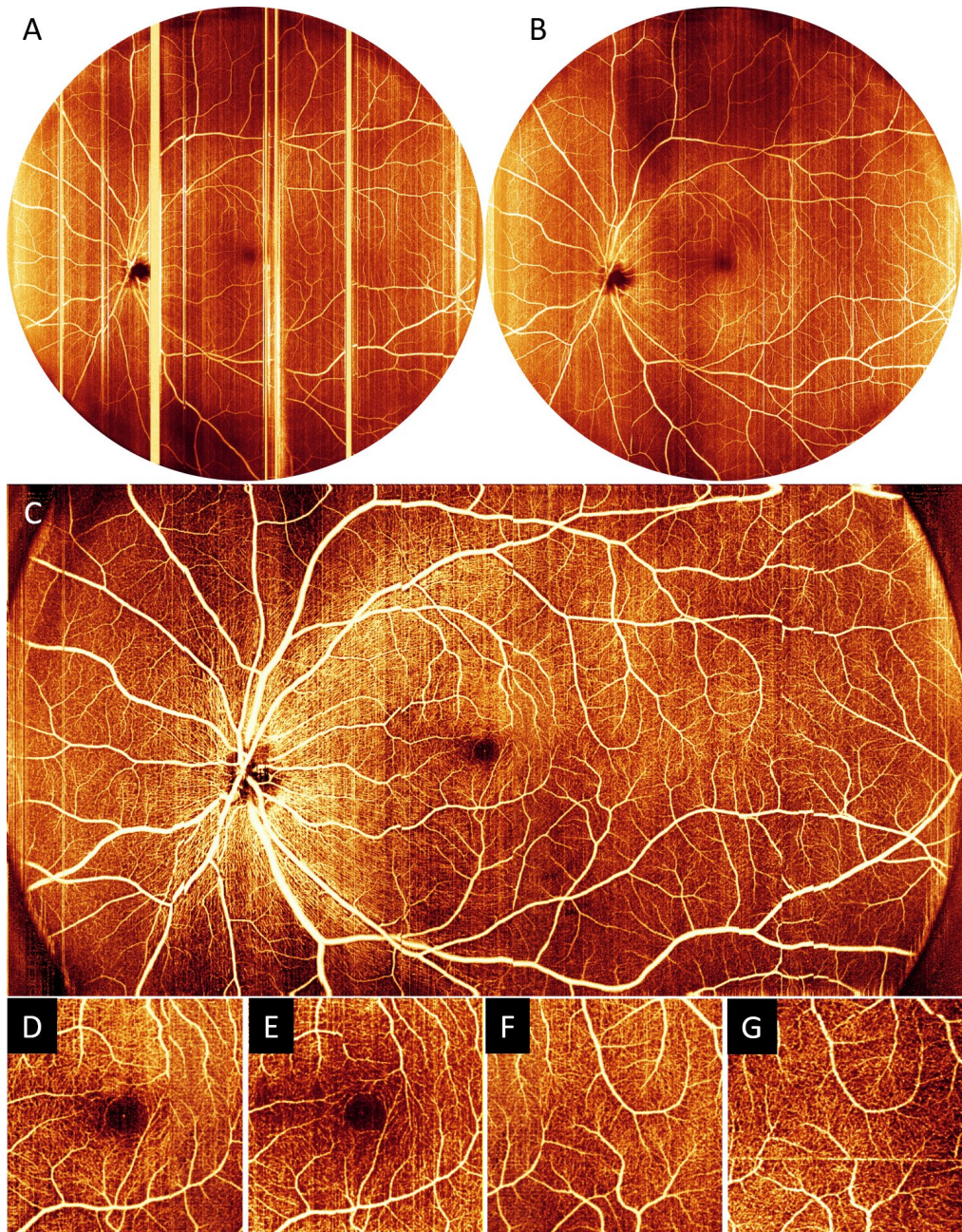


Figure 4, High-density wide-field OCTA images, (A) wide-field OCTA image acquired without tracking engaged, (B) wide-field OCTA image acquired with self-tracking engaged. The shadowing artifact is caused by eye lashes. (C) high-resolution wide-field OCTA image acquired with self-tracking engaged, (D, F)  $3 \times 3$  mm inner retinal image cropped from C, (E, G)  $3 \times 3$  mm inner retinal angiogram acquired using commercial system for comparison.

The same healthy subject's retinal image was acquired with horizontal 75-degree and vertical 38-degree FOV with the equivalent image size of  $23 \times 12$  mm. The image contained 1208 A-lines per B-scan, 2304 B-scans per volume with 3 repeated B-scans at each cross-sectional location for improving flow signal to noise ratio (SNR) and enhancing sampling density ( $10 \mu\text{m}/\text{line}$ ) on both horizontal and vertical axes. Our results demonstrated that the *en*

*face* OCTA (Fig. 4C) is free of blink and large motion artifacts, a few minor motion artifacts remain; the high sampling density enabled acquisition of high-resolution images with fine vascular details. For image quality comparison, the same healthy human subject was also scanned using a commercial OCT system (RTVue-XR Avanti; Optovue, Inc., Fremont, CA), with  $3 \times 3$  mm ( $304 \times 304$  lines) retinal images acquired in both the central macular region and the peripheral temporal area. For fair comparison, only the single-volume x-fast OCTA scans were used to generate the inner retinal *en face* images. We compared cropped images at the same position as the commercial scans from the high-resolution OCTA image (Fig. 4C). The images from the prototype system and the commercial system showed similar image quality and capillary visibility (Fig. 4D,E,F,G).

We also evaluated the performance of the tracking system quantitatively. We scanned 14 eyes from 7 healthy human subjects with and without the tracking system. The real-time OCTA *en face* images were generated along with the OCT spectrum raw data. Without the tracking system, 104 blinks were present across the images. With the tracking system, no blink artifacts were present in the images. The motion was measured automatically by calculating the IMSI, with the threshold is set to 0.25. Without tracking, 1,976 significant movements were detected. The tracking system reduced the number to 168; the automated system reduced the blinking and motion artifacts by 100% and 91.5% respectively.

#### *Patients with DR*

We acquired a  $23 \times 12$  mm OCTA from a 57-year-old female diagnosed with proliferative DR and early stage cataract. Our prototype system does not require dilation, but to minimize the difficulty of alignment during imaging the patient volunteer was dilated. The image disclosed areas of nonperfusion and dilated capillaries consistent with intraretinal microvascular abnormalities, revealing clinically relevant findings (Fig. 5).

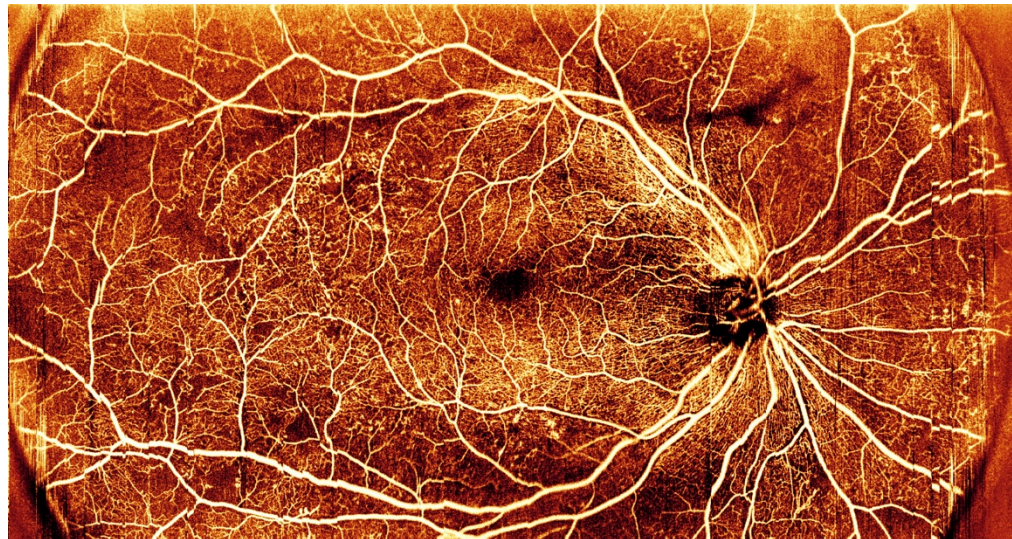


Figure 5. Inner retinal OCTA image acquired by our prototype from a proliferative diabetic retinopathy patient.

#### **4. Discussion**

In this paper, we present a novel OCTA-based motion and blink detection and tracking method that does not require additional hardware modification to an OCTA system. We applied this method to image both healthy and DR eyes, acquiring 75-degree wide-field capillary-level resolution OCTA with comparable capillary visibility to  $3 \times 3$  mm commercial OCTA images. To our knowledge, this is the first application of an OCTA based real-time self-tracking

application. Previously, OCT systems either used infrared fundus photography or infrared SLO as the reference for eye tracking and blink detection. The change in position of vessels in fundus images is the indicator of motion. Our system has several advantages over such conventional tracking methods. First, because no additional hardware is required, it reduces the complexity and cost of OCT systems; second, OCTA provides richer vasculature information to evaluate motion amplitude; third, fundus images are not adequately sensitive to small changes in vessel location to precisely align OCTA images due to their relatively low resolution. OCTA is intrinsically sensitive to movements (such as microsaccades) which make the detection of motion much easier than third party tracking methods.

GPU-based data processing technology accelerated the development of real-time OCT/OCTA. Our self-tracking method relies on high-speed, real-time OCTA image processing to respond to motion and blinking artifacts. The current bottleneck in real-time OCTA image processing is the data transfer speed. For real-time applications, the data transfer and processing time needs to be less than the data acquisition time. For our 400-kHz OCT system with 1204 A-lines per B-scan, a minimum of 12 B-scans needed to be batch processed together in a Nvidia RTX 2080ti GPU to maintain real-time processing. A larger batch can increase data processing efficiency at the cost of increased data transfer time. The tracking system must balance the processing efficiency and the tracking response time. A large batch will have a longer acquisition and processing time, which will result in a long response time. A slow response tracking system will directly extend the data acquisition time.

In our tracking system, one of the most important features is the IMSI. As the key motion indicator, the reliability of the IMSI directly correlated to the reliability of the tracking. Here, IMSI is a normalized value across several different B-scans. The normalization process removed the dependency on signal strength, yielding a pure correlation to motion. Thus, in our tracking algorithm, IMSI is independent to variation between different imaging subjects, different SNR and different types of systems. However, IMSI is still affected by the number of B-frames used in each batch. In our experience, a small batch rendered an unreliable IMSI. In our system, we used a high speed swept source laser, which requires at least 4 OCTA B-frames in each batch.

Wide-field OCTA imaging is challenging, and ocular pathology and involuntary motion can reduce image quality. Increasing the speed and sensitivity of the system can possibly overcome some of the difficulties. Many groups have applied high-speed swept source lasers [14, 30] to prototype OCT systems. One of the fastest swept wavelength laser sources is the Fourier domain mode lock (FDML) laser. It can achieve megahertz swept source rates. At such a high speed, video-rate OCT imaging has been realized [31]. In our system, we employed a 400-kHz rather than a megahertz swept source laser. There are several considerations when selecting a laser source. One is that increasing sweep rate decreases the SNR of the OCTA system. Another is the scanning speed. High scanning speeds require a resonant scanner. However, resonant scanners cause image distortion problems. Furthermore, high B-scan rates reduce the flow SNR and OCTA image quality due to diminished motion contrast. Finally, for wide-field imaging, a sufficient imaging range is required. For a 3-megahertz OCT system, suppose we need 1536 pixels per A-line. To acquire those pixels, a 5 GHz balanced detector is needed. However, currently it is a challenge to design such a balanced detector. All of these considerations explain our choice of the 400-kHz laser source.

Another challenge for wide-field OCTA imaging are shadows. In our previous study, a special optical system was designed to eliminate the shadow caused by the pupil and further reduce the shadowing problem [11]. This system was also employed in this work. The cross-scanning pattern applied in this work can also increase the alignment efficiency. Compared to the conventional multi-position method, the method presented here has a higher refresh rate that can show shadows in real-time. Doing so can help control scan quality.

Finally, we took advantage of GPU and SSADA processing efficiency. Together, these software and hardware improvements enabled the high-quality images presented in this work.

Our current tracking system still has some limitations. It can only provide an indicator that motion or blinking occurred, and does not provide any quantitative lateral or axial motion information. Without such information, the system is reliant on the fixation target and the cooperation of the patient to realign the eye after movement, which may introduce artifacts like vessel interruption.

## 5. Conclusion

We have successfully developed a real-time OCTA-based motion and blinking detection system for eye tracking. The tracking system is integrated in a wide-field high-speed swept-source OCT system capable of acquiring a 75-degree field-of-view high-density OCTA image in healthy and DR patients. By calculating an instantaneous motion index and rescanning in real time, the system detects and eliminates artifacts due to eye blinking and large movements. This system represents a significant improvement in field-of-view and resolution compared to a conventional OCT system.

## Funding

National Institutes of Health (R01 EY027833, R01 EY024544, P30 EY010572); unrestricted departmental funding grant and William & Mary Greve Special Scholar Award from Research to Prevent Blindness (New York, NY).

## Disclosures

Oregon Health & Science University (OHSU) and Yali Jia have a significant financial interest in Optovue, Inc. These potential conflicts of interest have been reviewed and managed by OHSU

## References

1. D. Huang, E. A. Swanson, C. P. Lin, J. S. Schuman, W. G. Stinson, W. Chang, M. R. Hee, T. Flotte, K. Gregory, C. A. Puliafito, and J. G. Fujimoto, "Optical coherence tomography," *science* **254**, 1178-1181 (1991).
2. S. Makita, Y. Hong, M. Yamanari, T. Yatagai, and Y. Yasuno, "Optical coherence angiography," *Optics express* **14**, 7821-7840 (2006).
3. Y. Jia, O. Tan, J. Tokayer, B. Potsaid, Y. Wang, J. J. Liu, M. F. Kraus, H. Subhash, J. G. Fujimoto, J. Horngger, and D. Huang, "Split-spectrum amplitude-decorrelation angiography with optical coherence tomography," *Optics express* **20**, 4710-4725 (2012).
4. L. An and R. K. Wang, "In vivo volumetric imaging of vascular perfusion within human retina and choroids with optical micro-angiography," *Optics Express* **16**, 11438-11452 (2008).
5. A. Mariampillai, B. A. Standish, E. H. Moriyama, M. Khurana, N. R. Munce, M. K. Leung, J. Jiang, A. Cable, B. C. Wilson, I. A. Vitkin, and V. X. D. Yang, "Speckle variance detection of microvasculature using swept-source optical coherence tomography," *Optics letters* **33**, 1530-1532 (2008).
6. L. A. Yannuzzi, K. T. Rohrer, L. J. Tindel, R. S. Sobel, M. A. Costanza, W. Shields, and E. Zang, "Fluorescein angiography complication survey," *Ophthalmology* **93**, 611-617 (1986).
7. Q. S. You, Y. Guo, J. Wang, X. Wei, A. Camino, P. Zang, C. J. Flaxel, S. T. Bailey, D. Huang, and Y. Jia, "Detection of clinically unsuspected retinal neovascularization with wide-field optical coherence tomography angiography," *Retina* (Philadelphia, Pa.) (2019).
8. R. G. Small and P. L. Hildebrand, "Preferred practice patterns," *Ophthalmology* **103**, 1987-1988 (1996).
9. T. Klein, W. Wieser, C. M. Eigenwillig, B. R. Biedermann, and R. Huber, "Megahertz OCT for ultrawide-field retinal imaging with a 1050nm Fourier domain mode-locked laser," *Optics express* **19**, 3044-3062 (2011).
10. L. R. De Pretto, E. M. Moult, A. Y. Alibhai, O. M. Carrasco-Zevallos, S. Chen, B. Lee, A. J. Witkin, C. R. Baumal, E. Reichel, A. Z. de Freitas, J. S. Duker, N. K. Waheed, and J. G. Fujimoto, "Controlling for Artifacts in Widefield Optical Coherence Tomography Angiography Measurements of Non-Perfusion Area," *Scientific Reports* **9**, 9096 (2019).
11. X. Wei, T. T. Hormel, Y. Guo, and Y. Jia, "75-degree non-mydriatic single-volume optical coherence tomographic angiography," *Biomedical Optics Express* **10**, 6286-6295 (2019).

12. Q. Zhang, C. S. Lee, J. Chao, C.-L. Chen, T. Zhang, U. Sharma, A. Zhang, J. Liu, K. Rezaei, K. L. Pepple, R. Munsen, J. Kinyoun, M. Johnstone, R. N. Van Gelder, and R. K. Wang, "Wide-field optical coherence tomography based microangiography for retinal imaging," *Scientific reports* **6**, 22017 (2016).
13. R. F. Spaide, J. G. Fujimoto, and N. K. Waheed, "Image artifacts in optical coherence angiography," *Retina* (Philadelphia, Pa.) **35**, 2163 (2015).
14. W. Wieser, B. R. Biedermann, T. Klein, C. M. Eigenwillig, and R. Huber, "Multi-megahertz OCT: High quality 3D imaging at 20 million A-scans and 4.5 GVOXels per second," *Optics express* **18**, 14685-14704 (2010).
15. Z. Zhi, W. Qin, J. Wang, W. Wei, and R. K. Wang, "4D optical coherence tomography-based microangiography achieved by 1.6-MHz FDML swept source," *Optics letters* **40**, 1779-1782 (2015).
16. J. Xu, C. Zhang, J. Xu, K. Wong, and K. Tsia, "Megahertz all-optical swept-source optical coherence tomography based on broadband amplified optical time-stretch," *Optics letters* **39**, 622-625 (2014).
17. J. Kang, P. Feng, X. Wei, E. Y. Lam, K. K. Tsia, and K. K. Wong, "102-nm, 44.5-MHz inertial-free swept source by mode-locked fiber laser and time stretch technique for optical coherence tomography," *Optics express* **26**, 4370-4381 (2018).
18. P. Zang, G. Liu, M. Zhang, C. Dongye, J. Wang, A. D. Pechauer, T. S. Hwang, D. J. Wilson, D. Huang, D. Li, and Y. Jia, "Automated motion correction using parallel-strip registration for wide-field en face OCT angiogram," *Biomedical optics express* **7**, 2823-2836 (2016).
19. A. Camino, Y. Jia, G. Liu, J. Wang, and D. Huang, "Regression-based algorithm for bulk motion subtraction in optical coherence tomography angiography," *Biomedical optics express* **8**, 3053-3066 (2017).
20. J. Wang, A. Camino, X. Hua, L. Liu, D. Huang, T. S. Hwang, and Y. Jia, "Invariant features-based automated registration and montage for wide-field OCT angiography," *Biomedical optics express* **10**, 120-136 (2019).
21. Y. Li, G. Gregori, B. L. Lam, and P. J. Rosenfeld, "Automatic montage of SD-OCT data sets," *Optics express* **19**, 26239-26248 (2011).
22. Y. Cui, Y. Zhu, J. C. Wang, Y. Lu, R. Zeng, R. Katz, D. M. Wu, D. G. Vavvas, D. Husain, and J. W. Miller, "Imaging Artifacts and Segmentation Errors With Wide-Field Swept-Source Optical Coherence Tomography Angiography in Diabetic Retinopathy," *Translational Vision Science & Technology* **8**, 18-18 (2019).
23. K. V. Virola, B. Braaf, C. K. Sheehy, Q. Yang, P. Tiruveedhula, D. W. Arathorn, J. F. de Boer, and A. Roorda, "Real-time eye motion compensation for OCT imaging with tracking SLO," *Biomedical optics express* **3**, 2950-2963 (2012).
24. R. D. Ferguson, D. X. Hammer, L. A. Paunescu, S. Beaton, and J. S. Schuman, "Tracking optical coherence tomography," *Optics letters* **29**, 2139-2141 (2004).
25. D. X. Hammer, R. D. Ferguson, N. V. Iftimia, T. Ustun, G. Wollstein, H. Ishikawa, M. L. Gabriele, W. D. Dilworth, L. Kagemann, and J. S. Schuman, "Advanced scanning methods with tracking optical coherence tomography," *Optics express* **13**, 7937-7947 (2005).
26. A. F. Fercher, W. Drexler, C. K. Hitzenberger, and T. Lasser, "Optical coherence tomography-principles and applications," *Reports on progress in physics* **66**, 239 (2003).
27. X. Wei, A. Camino, S. Pi, T. T. Hormel, W. Cepurna, D. Huang, J. C. Morrison, and Y. Jia, "Real-time cross-sectional and en face OCT angiography guiding high-quality scan acquisition," *Optics letters* **44**, 1431-1434 (2019).
28. Y. Guo, A. Camino, M. Zhang, J. Wang, D. Huang, T. Hwang, and Y. Jia, "Automated segmentation of retinal layer boundaries and capillary plexuses in wide-field optical coherence tomographic angiography," *Biomedical optics express* **9**, 4429-4442 (2018).
29. T. T. Hormel, J. Wang, S. T. Bailey, T. S. Hwang, D. Huang, and Y. Jia, "Maximum value projection produces better en face OCT angiograms than mean value projection," *Biomedical optics express* **9**, 6412-6424 (2018).
30. J. Xu, X. Wei, L. Yu, C. Zhang, J. Xu, K. Wong, and K. K. Tsia, "High-performance multi-megahertz optical coherence tomography based on amplified optical time-stretch," *Biomedical optics express* **6**, 1340-1350 (2015).
31. J. P. Kolb, W. Draxinger, J. Klee, T. Pfeiffer, M. Eibl, T. Klein, W. Wieser, and R. Huber, "Live video rate volumetric OCT imaging of the retina with multi-MHz A-scan rates," *PLoS one* **14**, e0213144 (2019).